

Non-Compact QED₃ with $N_f = 1$ and $N_f = 4$

S.J. Hands^{a,b}, J.B. Kogut^c, L. Scorzato^d and C.G. Strouthos^{e,f}

^a *Department of Physics, University of Wales Swansea,
Singleton Park, Swansea, SA2 8PP, U.K.*

^b *Institute for Nuclear Theory, University of Washington,
Box 351550, Seattle WA 98195, U.S.A.*

^c *Department of Physics, University of Illinois at Urbana-Champaign,
Urbana, IL 61801-3080, U.S.A.*

^d *Institut für Physik, Humboldt Universität zu Berlin, 12489 Berlin, Germany,*

^e *Department of Physics, Duke University, Durham, NC 27708, U.S.A.*

^f *Division of Science and Engineering, Frederick Institute of Technology,
Nicosia 1303, Cyprus.*

Abstract

We present numerical results for non-compact three-dimensional QED for numbers of flavors $N_f = 1$ and $N_f = 4$. In particular, we address the issue of whether chiral symmetry is spontaneously broken in the continuum limit, and obtain a positive answer for $N_f = 1$, with a dimensionless condensate estimated to be $\beta^2 \langle \bar{\psi} \psi \rangle \simeq O(10^{-3})$, implying that the critical number of flavors $N_{fc} > 1$. We also compare the $N_f = 1$ and $N_f = 4$ models by analysing the transition from strong to weak coupling behaviour using an equation of state based on a continuous phase transition. While some qualitative differences emerge, it appears difficult to determine whether $N_f = 4$ lies above or below N_{fc} .

1 Introduction and Motivation

The nature of the ground state of Quantum Electrodynamics in 2+1 dimensions and its dependence on the number of fermion species N_f has been an important problem for non-perturbative field theorists for 20 years [1]. The question is the value of critical number of flavors N_{fc} such that for $N_f < N_{fc}$ the theory's chiral symmetry is spontaneously broken, resulting in a dynamically generated mass for the fermion. Over the years the main method of attack has been to solve the Schwinger-Dyson equation for the fermion self-energy $\Sigma(k)$, to see if $\lim_{k \rightarrow 0} \Sigma(k) \neq 0$; this has resulted in a variety of predictions for N_{fc} ranging between $32/\pi^2$ and ∞ , with most recent attempts yielding $N_{fc} \simeq 4$ [2]. Over the same period there have also been attempts to decide the issue by numerical simulation of non-compact lattice QED [3, 4, 5]. Numerical approaches are hindered by large finite volume effects, and the intrinsic smallness of the relevant signal, the so-called dimensionless condensate $\beta^2 \langle \bar{\psi} \psi \rangle$ (to be defined in what follows) in the continuum limit: in a recent study [6] of the model with $N_f = 2$ we placed an upper bound on this quantity of $O(10^{-4})$, but even this does not exclude the predictions of some self-consistent approaches with $N_{fc} > 2$ [7, 8].

Interest in the problem has recently been revived by the suggestion that QED₃ may be an effective theory for the underdoped and non-superconducting region of the phase diagram of high- T_c superconducting cuprate compounds [9, 10]. In brief, superconductivity in these substances is confined to planes defined by CuO₂ layers, thus motivating a 2+1d description. The superconducting order parameter has a d -wave symmetry, implying that there are four nodes in the gap function $\Delta(\vec{k})$ as the Fermi surface (which in 2+1d is a curve) is circumnavigated. At each node the low-energy quasiparticle excitations obey an approximately linear dispersion relation $E(\vec{k}) \propto |\vec{k} - \vec{k}_{node}|$, with the result that it is possible to rewrite the action for eight distinct low energy species (spin up and spin down at each of four nodes) in a relativistically invariant form in terms of $N_f = 2$ species of four-component Dirac spinor¹. The next link in the chain is the observation that disruption of superconducting order in a planar system occurs via condensation of vortex singularities in the phase ϕ of the U(1)-valued order parameter, while $|\Delta|$ remains unchanged. Because the order parameter field is doubly charged since it arises from electron pairing, in the presence of a distribution of vortices it is impossible in general to reabsorb ϕ into the definition of the quasiparticle fields while leaving their wavefunction single-valued. There is, however, a particular gauge [11] in which the problem can be recast in terms of single-valued quasiparticle fields interacting with a real-valued vector field. The component of the vector field that is minimally coupled to the quasiparticles remains massless under quantum corrections (vacuum polarisation due to virtual particle hole pairs), and is identified with the photon of QED₃². It is then argued [9, 10] that the effective action for the photon fluctuations is of the non-compact form $F_{\mu\nu}^2$, with an effective “electric charge” coupling photons to quasiparticles proportional to the vortex disorder parameter, which is non-zero as soon as vortices unbind, ie. *outside* the superconducting region of the phase diagram.

¹For phenomenologically relevant models the action for each individual flavor exhibits a spatial anisotropy, a feature ignored in this paper.

²In fact, the photon can be regarded as the Goldstone boson associated with vortex condensation [12].

If QED₃ is a relevant effective theory for cuprates, then the abstract theoretical problem of the value of N_{fc} assumes concrete phenomenological reference. If $N_{fc} > 2$, then the theory is chirally broken at zero temperature. On retranslating from the Dirac spinor basis to the original electron degrees of freedom, the chiral order parameter is reinterpreted as an order parameter for spin density waves, whose wavevector gets shorter and shorter as doping is decreased, until at zero doping the Néel antiferromagnetic state is recovered [10]. This picture therefore predicts the existence of a phase boundary between superconducting (dSC) and antiferromagnetic (AFM) phases at some non-zero doping in the zero temperature limit. If, on the other hand, $N_{fc} < 2$, the chirally symmetric ground state manifests itself as a tongue of “pseudogap” phase separating dSC from AFM, in which normal Fermi liquid properties may be modified as a result of a non-perturbative anomalous dimension for the fermion field [9].

In order to motivate further study, let us review two arguments concerning N_{fc} which are independent of Schwinger-Dyson analyses. A recent discussion of similar issues can be found in [7]. The first due, to Appelquist, Cohen and Schmaltz [13], postulates an inequality

$$f_{IR} \leq f_{UV} \quad (1)$$

between thermodynamic free energy densities (ie. pressures) due to the weakly-interacting degrees of freedom characteristic of respectively long and short distance regimes. Since f is simply related to the number of weakly interacting degrees of freedom, this can be easily checked for QED₃. In the UV limit $f_{UV} \propto 1 + \frac{3}{4}(4N_f)$, where 1 counts the photon, which has only one physical polarisation in 2+1d, and the second term, which includes a numerical factor arising from Fermi-Dirac statistics, counts free fermions. In the IR limit for $N_f < N_{fc}$ there is still a photon, but chiral symmetry breaking $U(2N_f) \rightarrow U(N_f) \otimes U(N_f)$ implies $2N_f^2$ Goldstone modes, so $f_{IR} \propto 1 + 2N_f^2$. Eqn. (1) then yields the bound $N_{fc} \leq \frac{3}{2}$. It should be pointed out, however, that this argument may not be applicable to a 2+1d system, since in this low dimensionality bosonic modes exhibit strong fluctuations and hence are never weakly interacting [14].

Another argument starts from the similarity between QED₃ and the 2+1 dimensional Thirring model defined by the Lagrangian

$$\mathcal{L}_{Thir} = \bar{\psi}_i(\not{\partial} + m)\psi_i + \frac{G^2}{2N_f}(\bar{\psi}_i\gamma_\mu\psi_i)^2. \quad (2)$$

In the limit $G^2 \rightarrow \infty$ there is a massless vector meson, ie. a $\psi\bar{\psi}$ bound state with the same quantum numbers as the photon; moreover both models have identical quantum corrections when calculated in an expansion in powers of N_f^{-1} [15]. However, the resemblance may also be non-perturbative in N_f^{-1} ; Itoh *et al* [16] pointed out that in a certain non-local gauge the self-consistent gap equation for chiral symmetry breaking in the Thirring model coincides in the limit $G^2 \rightarrow \infty$ with that of QED₃, implying a vanishing chiral order parameter for some critical N'_{fc} . In the Thirring case, however, the vanishing of the gap also happens for $N_f < N'_{fc}$, $G^2 = G_c^2 < \infty$, and signals a UV fixed point of the renormalisation group at which a non-trivial continuum limit may be taken. This picture has received support from

numerical simulations with finite N_f , which suggest that $4 < N'_{fc} < 6$ [17, 18, 19]. Since the pattern of global symmetry breaking is the same for both models, it is tempting to postulate that the IR fixed point behaviour of QED₃ coincides with the UV behaviour of Thirring in the $G^2 \rightarrow \infty$ limit, and hence $N_{fc} = N'_{fc} \sim 5$.

Since neither argument is obviously nonsense, and since they yield predictions for N_{fc} which differ significantly both from each other and from the Schwinger-Dyson approach, it is clear that consensus on this issue has yet to emerge, and that further numerical efforts are justified. In [6] we were unable to find any signal for chiral symmetry breaking, but also unfortunately were not able to definitively exclude it being present with the tiny value predicted in the self-consistent approach [7, 8]. In this paper we build on that work by performing extensive simulations of non-compact QED₃ with $N_f = 1$ and $N_f = 4$, the hope being that if these two values were to straddle N_{fc} , then some difference in their behaviour, either quantitative or qualitative, may show up. The lattice formulation and simulation method is reviewed in the next section, and the numerical results presented in Sec. 3. We shall see that for $N_f = 1$ there is convincing evidence for broken chiral symmetry, implying $N_{fc} > 1$; unfortunately, while we can uncover some qualitative differences between $N_f = 1$ and $N_f = 4$, there is no decisive evidence that they have different ground states in the continuum limit.

2 The Model and the Simulation

The action of the lattice model we study is

$$\begin{aligned}
S &= \frac{\beta}{2} \sum_{x, \mu < \nu} \Theta_{\mu\nu}(x) \Theta_{\mu\nu}(x) + \sum_{i=1}^N \sum_{x, x'} \bar{\chi}_i(x) M(x, x') \chi_i(x') \quad (3) \\
\Theta_{\mu\nu}(x) &\equiv \theta_{x\mu} + \theta_{x+\hat{\mu}, \nu} - \theta_{x+\hat{\nu}, \mu} - \theta_{x\nu} \\
M(x, x') &\equiv m_0 \delta_{x, x'} + \frac{1}{2} \sum_{\mu} \eta_{\mu}(x) [\delta_{x', x+\hat{\mu}} U_{x\mu} - \delta_{x', x-\hat{\mu}} U_{x-\hat{\mu}, \mu}^{\dagger}].
\end{aligned}$$

This describes interactions between N flavors of Grassmann-valued staggered fermion fields $\chi, \bar{\chi}$ defined on the sites x of a three-dimensional cubic lattice, and real photon fields $\theta_{x\mu}$ defined on the link between nearest neighbour sites $x, x + \hat{\mu}$. Since Θ^2 is unbounded from above, (3) defines a non-compact formulation of QED; note however that to ensure local gauge invariance the fermion-photon interaction is encoded via the compact connection $U_{x\mu} \equiv \exp(i\theta_{x\mu})$, with $U_{x+\hat{\mu}, -\mu} = U_{x\mu}^*$. In the fermion kinetic matrix M the Kawamoto-Smit phases

$$\eta_{\mu}(x) = (-1)^{x_1 + \dots + x_{\mu-1}} \quad (4)$$

are designed to ensure relativistic covariance in the continuum limit, and m_0 is the bare fermion mass.

If the physical lattice spacing is denoted a , then in the continuum limit $a\partial \rightarrow 0$, (3) can

be shown to be equivalent up to terms of $O(a^2)$ to

$$S = \sum_{j=1}^{N_f} \bar{\psi}^j [\gamma_\mu (\partial_\mu + igA_\mu) + m] \psi^j + \frac{1}{4} F_{\mu\nu} F_{\mu\nu} \quad (5)$$

ie. to continuum QED in 2+1 euclidean dimensions, with $\psi, \bar{\psi}$ describing N_f flavors of 4 component Dirac spinor acted on by 4×4 matrices γ_μ , and $N_f \equiv 2N$. The continuum photon field is related to the lattice field via $\theta_{x\mu} = agA_\mu(x)$, with dimensional coupling strength g given by $g^2 = (a\beta)^{-1}$, and the field strength $F_{\mu\nu} = \partial_\mu A_\nu - \partial_\nu A_\mu$. The continuum limit is thus taken when the dimensionless inverse coupling $\beta \rightarrow \infty$.

As reviewed in [6], for $a > 0$ in the chiral limit the lattice action (3) retains only a remnant of the $U(2N_f)$ global symmetry of (5) under global chiral/ flavor rotations, namely a $U(N) \otimes U(N)$ symmetry which is broken to $U(N)$ either explicitly by the bare mass $m \neq 0$, or spontaneously by a chiral condensate $\langle \bar{\chi}\chi \rangle \neq 0$, in which case the spectrum contains N^2 exact Goldstone modes. It is expected that the symmetry breaking pattern $U(2N_f) \rightarrow U(N_f) \otimes U(N_f)$ is restored in the continuum limit, implying the existence of an additional $7N^2$ approximate Goldstone modes whose masses vanish as $\beta \rightarrow \infty$.

The simulations in this paper were performed using two different algorithms. The model with $N_f = 4$ is studied by exact simulations of the action (3) with $N = 2$ using the hybrid Monte Carlo algorithm, exactly as done for $N_f = 2$ in [6]. The model with $N_f = 1$ is simulated using $\det^{\frac{1}{2}} M$ as a functional measure using a hybrid molecular dynamics R algorithm [20], which generates a Markov chain of representative configurations by evolution of a system of stochastic differential equations with timestep $\Delta\tau$. The algorithm has a systematic error $\propto N^2 \Delta\tau^2$; in our work we use values of $\Delta\tau$ ranging from 0.1 down to 0.0025, the value required getting smaller as β decreases, L_s increases, and m_0 decreases, and have checked that this is sufficient to render systematic errors smaller than statistical ones. Beyond this technical point, however, we should point out the conceptual issue that simulations with fractional N do not reproduce the physics of a local fermion bilinear action except in the deep continuum limit when flavor symmetries are restored. It remains an open issue within the lattice QCD community whether this is a source of significant systematic error at achievable lattice spacings [21]. Whilst we make no attempt to address this issue in the current study, we should not exclude the possibility that delayed flavor symmetry restoration could lead to a misleading prediction for the ground state properties at finite β [6]. In Sec. 3.2 below we shall present evidence for flavor symmetry violating effects of just $O(10\%)$ at the weakest couplings examined.

To check if chiral symmetry is broken in continuum QED₃, we need to establish whether, on a system of finite extent $L = L_s \times a$

$$\lim_{\beta \rightarrow \infty} \lim_{\beta m_0 \rightarrow 0} \lim_{L_s / \beta \rightarrow \infty} \beta^2 \langle \bar{\chi}\chi \rangle \neq 0. \quad (6)$$

The order of limits is important: since a continuous symmetry never breaks spontaneously on a finite volume we must always work with $m \neq 0$, and only attempt to take the chiral limit once the thermodynamic limit is reached. Since for an asymptotically-free theory like QED₃

the UV behaviour is governed by the gaussian fixed point at the origin, all physical quantities are expressible in terms of the scale set by g , and hence to compare data taken at different lattice spacings, it is natural to use the combinations βm_0 , L_s/β and $\beta^2 \langle \bar{\chi}\chi \rangle$ corresponding to the dimensionless combinations m/g^2 , Lg^2 , and $g^{-4} \langle \bar{\psi}\psi \rangle$. As the continuum limit is approached data taken at different β should collapse onto a universal curve when plotted in these units.

Taking all three limits of equation (6) is extremely demanding computationally, as revealed in [6], where in practise we were only able to place an upper bound on the condensate for $N_f = 2$ of $\beta^2 \langle \bar{\chi}\chi \rangle \leq 5 \times 10^{-5}$. The small size of the dimensionless condensate in this case implies that a large separation of scales $\xi \gg a$ may be taking place, and therefore a much larger infra-red cutoff $L \gg \xi$ required to probe chiral symmetry breaking if it is indeed present [22]. The small number is not, however, inconsistent with current estimates based on solutions of the Schwinger-Dyson equations [7, 8]. It therefore appears unlikely that the critical value N_{fc} can be established using current computational resources if $N_{fc} > 2$.

In this paper our aims are twofold. First, since the self-consistent solutions suggest an exponential suppression $\langle \bar{\psi}\psi \rangle \sim \exp(-f(N_f))$, where f is an increasing function of N_f for $N_f < N_{fc}$, the dimensionless condensate for $N_f = 1$ may well be much larger and hence easier to measure using current resources. Secondly, we will look for qualitative differences between data taken with $N_f = 1$ and $N_f = 4$ to see what evidence if any can be found that they lie on opposite sides of N_{fc} , by fitting the condensate data to a global equation of state based on a chiral symmetry restoring transition at finite $\beta_c(N_f)$. For $N_f < N_{fc}$ this ‘‘critical’’ coupling need not correspond to a true phase transition, but instead could mark a crossover from strong to weak-coupling behaviour.

3 Simulation Results

For $N_f = 1$ we have results from lattice volumes 24^3 ($0.25 \leq \beta \leq 0.45$), 32^3 ($0.45 \leq \beta \leq 0.65$), 44^3 ($\beta = 0.55$), 48^3 ($\beta = 0.65$), and in addition five studies at $\beta = 0.90$ on 16^3 , 24^3 , 36^3 , 54^3 and 80^3 . For $N_f = 4$ we have 16^3 ($0.15 \leq \beta \leq 0.2$), 24^3 ($0.15 \leq \beta \leq 0.225$), 32^3 ($0.4 \leq \beta \leq 0.6$), and 48^3 ($\beta = 0.4$). For the most part we examined mass values in the range $0.003 \leq m_0 \leq 0.025$. For each parameter set we took typically 200 - 300 trajectories of mean length $\bar{\tau} = 1.0$. Several different computing facilities were used, so an estimate of the cpu resource required is approximate at best, but a figure of 12 months running on a cluster of 30 1.2 GHz processors is not unreasonable. In Figs. 1 ($N_f = 1$) and 2 ($N_f = 4$) we show the datasets thus obtained for $\langle \bar{\chi}\chi \rangle$ as a function of β and m_0 . The lines are fits to a global equation of state to be described in Sec. 3.3.

3.1 Chiral Condensate in Chiral and Continuum Limits

In an attempt to get an overview of the model’s behaviour, for each β and N_f we first attempt an extrapolation to the chiral limit of the form

$$\langle \bar{\chi}\chi \rangle = \langle \bar{\chi}\chi \rangle_0 + Am_0 + Bm_0^{\frac{3}{2}} \quad (7)$$

and plot the resulting $\langle\bar{\chi}\chi\rangle_0$ as a function of β in Fig. 3. We have checked that at least at stronger couplings where the signal is appreciable the results are relatively insensitive to changes in the extrapolation function, eg. to incorporate non-analyticities due to Goldstone degrees of freedom [23]. We see that for both N_f values chiral symmetry clearly appears to be broken at strong coupling, but that $\langle\bar{\chi}\chi\rangle_0$ decreases as β is increased, so that we can identify either a crossover or a symmetry restoring phase transition at $\beta \simeq 0.5$ ($N_f = 1$) or $\beta \simeq 0.25$ ($N_f = 4$). Global fits to the data will be used in Sec. 3.3 to explore the nature of these points further. There is some evidence already from Fig. 3 that the curvature of $\langle\bar{\chi}\chi\rangle_0(\beta)$ differs between the two values of N_f , a feature already noted in [3].

In an attempt to see whether chiral symmetry is broken in the continuum limit $\beta \rightarrow \infty$ we compare plots of the dimensionless variables $\beta^2\langle\bar{\chi}\chi\rangle$ versus βm_0 for different N_f in Fig. 4. The data for $N_f = 2$ are from [6], where it was concluded that when extrapolated to the continuum limit $\beta^2\langle\bar{\chi}\chi\rangle \lesssim 10^{-4}$. By comparing $N_f = 1, 2$ and 4 one sees that increasing N_f at fixed βm_0 suppresses the condensate, as might be expected due to enhanced screening from virtual $\chi\bar{\chi}$ pairs. There is clearly no prospect of finding a signal for chiral symmetry breaking with $N_f = 4$ with this dataset. The $N_f = 1$ data, however, are significantly larger near the chiral limit.

In Fig. 5 we show the plot for $N_f = 1$ zoomed in the neighbourhood of the origin for two different lattice spacings each with two volumes. The smaller of the two $\beta = 0.90$ lattices is intermediate in physical volume between the two $\beta = 0.65$ lattices, whereas the $\beta = 0.90$ 80^3 data is closest to both continuum and thermodynamic limits. There are clear finite volume effects at both lattice spacings for $\beta m_0 < 0.005$. By comparing $\beta = 0.65$ with $\beta = 0.90$ it is clear there are also still lattice discretisation artifacts of $O(10\%)$. A linear fit to data on the larger volume extrapolates to a chiral limit value $\beta^2\langle\bar{\chi}\chi\rangle = 0.0041(4)$ for $\beta = 0.65$ (fit to the lowest 5 mass points), and $0.0043(2)$ for $\beta = 0.90$, with the fitted slopes differing by about $20\%^3$. Due to finite volume effects these numbers are if anything underestimates. Therefore whilst it is premature to quote a value for the dimensionless condensate due to lack of control over systematic errors, we are confident in claiming that it is $\gtrsim 10^{-3}$, ie. greater than zero, almost two orders of magnitude greater than the upper bound quoted for $N_f = 2$ in [6], and very roughly half the result for $N_f = 0$ (ie. quenched QED₃) found in [5]. Note, moreover, that our lowest mass datapoint at $\beta = 0.90$ has $\beta^2\langle\bar{\chi}\chi\rangle$ only three times its value in the chiral limit, making the linear extrapolation of Fig. 5 considerably less adventurous than those of [5]. Any extrapolation which obtains a significantly smaller result in the chiral limit must be based on an analytic form which curves sharply as the chiral limit is approached. One possible form is $\langle\bar{\chi}\chi\rangle = a_0 + a_1 m_0^{\frac{1}{2}} + \dots$, predicted by the effective chiral theory describing the influence of pion fluctuations (see eg. [23]). The applicability of such a model, however, presupposes chiral symmetry breaking. Our conclusion that $N_{fc} > 1$ is probably quite robust.

³Note that the slope of the line corresponds to the longitudinal susceptibility $\chi_l = \partial^2 \ln Z / \partial m_0^2$, which as a two-point function is expected to be more severely finite-volume affected.

3.2 Meson Spectroscopy

A physically meaningful way of assessing how far the simulations lie from the continuum limit comes by checking the degree of flavor symmetry restoration in the meson spectrum. Recall that in the continuum theory with $N_f = 2$ [24], chiral symmetry breaking $U(4) \rightarrow U(2) \otimes U(2)$ results in eight Goldstone bosons, which somewhat sloppily we will continue to refer to as “pions”. If we denote the Euclidean time direction as x_3 , then the pion states can be divided into 4 pseudoscalars $\bar{\psi}(\gamma_5 \otimes \mathbf{1})\psi$, $\bar{\psi}(\gamma_5 \otimes \tau_i)\psi$ and 4 scalars $\bar{\psi}(\gamma_4 \otimes \mathbf{1})\psi$, $\bar{\psi}(\gamma_4 \otimes \tau_i)\psi$, where $\{\mathbf{1}_2, \vec{\tau}\}$ generate a $U(2)$ symmetry acting on flavor indices. In the lattice model the corresponding states in terms of staggered fermions read [25]:

$$\bar{\psi}(\gamma_5 \otimes \mathbf{1})\psi \Leftrightarrow \bar{\chi}(x)\chi(x)\varepsilon(x); \quad (8)$$

$$\bar{\psi}(\gamma_4 \otimes \tau_\mu)\psi \Leftrightarrow \bar{\chi}(x)\chi(x + \hat{\mu})\varepsilon(x)\zeta_\mu(x); \quad (9)$$

$$\bar{\psi}(\gamma_5 \otimes \tau_\mu)\psi \Leftrightarrow |\epsilon_{\mu\nu\lambda}|\bar{\chi}(x)\chi(x + \hat{\nu} + \hat{\lambda})\varepsilon(x)\zeta_\nu(x)\zeta_\lambda(x); \quad (10)$$

$$\bar{\psi}(\gamma_4 \otimes \mathbf{1})\psi \Leftrightarrow |\epsilon_{\mu\nu\lambda}|\bar{\chi}(x)\chi(x + \hat{\mu} + \hat{\nu} + \hat{\lambda}), \quad (11)$$

where we have defined additional phase factors $\varepsilon(x) = (-1)^{x_1+x_2+x_3}$, $\zeta_\mu(x) = \varepsilon(x)\eta_\mu(x)(-1)^{x_\mu}$, and an average over forward and backward link shifts is understood. The parity operation for staggered fermions with the definition (4) for the Kawamoto-Smit phases is

$$x = (x_1, x_2, x_3) \mapsto x' = (1 - x_1, x_2, x_3) \quad ; \quad \chi(x) \mapsto \varepsilon(x')\chi(x'), \quad \bar{\chi}(x) \mapsto \varepsilon(x')\bar{\chi}(x') \quad (12)$$

The assignment of scalar and pseudoscalar labels to the states is readily checked.

Spectroscopy on the lattice through decay of temporal correlation functions is most transparent when restricted to operators defined on a single timeslice. This means that in addition to the state (8) which interpolates an exact Goldstone state for the residual lattice chiral symmetry breaking $U(1) \otimes U(1) \rightarrow U(1)$, it is possible to examine two scalar states interpolated by one-link operators (9) and one pseudoscalar interpolated by a two-link operator (10). At non-zero lattice spacing these latter states are not associated with Goldstones of an exact symmetry, and the degeneracy between the states expected in the continuum limit is split by terms which are generically $O(a)$. The extent to which the measured masses are degenerate, therefore, gives some measure of the approach to the continuum limit. Note that flavor symmetry restoration should still manifest itself in this fashion even if chiral symmetry is unbroken, since in this case the various states are related by $U(2) \otimes U(2)$ rotations.

We have tested the approach to the continuum limit for $N_f = 1$ by measuring the masses of the local, 1-link and 2-link pions at $\beta = 0.6, 0.75$ and 0.9 with fixed values of $\beta m_0 = 0.0009$ and $L_s/\beta = 40$. In this way any systematic errors due to eg. finite volume should cancel. The results are plotted in Fig. 6. Whilst the data is still too noisy to determine the level ordering unequivocally, we can see that the splitting of 40% at $\beta = 0.6$ is reduced to 15% by $\beta = 0.9$, which thus gives a sample estimate for the residual systematic errors due to lattice artifacts at this closest approach to the continuum limit.

3.3 Global Fits to Equation of State

In this section we change tack, retreating from direct attempts to probe the continuum limit, and instead exploiting the data at stronger couplings to make qualitative statements about the behaviour as a function of N_f . In the strong coupling limit $\beta \rightarrow 0$, it is known rigorously that chiral symmetry is spontaneously broken [26], and indeed our data confirm this (see Figs. 1,2). Therefore as β increases, for $N_f > N_{fc}$ there must be a chiral symmetry restoring phase transition for some finite β_c . For $N_f < N_{fc}$, since we believe the order parameter is exponentially small in the continuum limit, the relic of this transition may persist as a crossover between strong and weak coupling behaviour, much as in lattice QCD. For N_f exactly equal to N_{fc} , the order parameter should vanish in the chiral continuum limit, but with a non-analytic response to a small bare mass of the form $\langle \bar{\chi}\chi \rangle \propto m_0^\delta$, a behaviour characteristic of a so-called “conformal fixed point” [27, 24].

We therefore proceed with the assumption (which must be unphysical for $N_f < N_{fc}$) that there is a continuous chiral symmetry-restoring phase transition described by the following equation of state:

$$m_0 = A(\beta - \beta_c)\langle \bar{\chi}\chi \rangle^p + B\langle \bar{\chi}\chi \rangle^\delta, \quad (13)$$

and attempt to fit the entire dataset, or at least a significant fraction, for each N_f . Eqn. 13 has 5 free parameters, the “critical” coupling β_c , exponents δ and p , and the amplitudes A and B . Setting $\beta = \beta_c$ shows that δ has its conventional interpretation as a critical exponent describing response of an order parameter to an external field, and setting $m_0 = 0$ shows that the conventional exponent describing scaling of the order parameter in the broken symmetry phase is given by $\beta_{mag} = (\delta - p)^{-1}$. The fits are performed using the MINUIT package.

For $N_f = 1$ there are a total of 151 points in the dataset (excluding $\beta = 0.9$). The best fit found was to the 109 points with $0.25 \leq \beta \leq 0.45$ using data from all masses and from the largest available volume at any given β . This gives

$$\begin{aligned} A &= 4.43(17) & \delta &= 2.33(4) & \beta_c &= 0.451(4) & \chi^2/dof &= 1.02 \\ B &= 1.87(7) & p &= 1.50(2) \end{aligned} \quad (14)$$

Acceptable fits persist, with little change in the parameters, if data with $\beta = 0.400, 0.450$ is excluded. The χ^2/dof increases to 1.5 if $\beta = 0.55$ is included, and 2.5 if $\beta = 0.65$ is included, once again with relatively little impact on the fit parameters. If instead strong coupling data with $\beta \leq 0.40$ are excluded, then χ^2/dof rises to $\gtrsim 4$, and the fitted values of δ and p drift downwards.

The raw data are plotted with the fit (14) in Fig. 1, and the fit is also shown in “Fisher coordinates” for strong (Fig. 7) and weak (Fig. 8) coupling data. The Fisher plot of $\langle \bar{\chi}\chi \rangle^2$ versus $m_0/\langle \bar{\chi}\chi \rangle$ is devised so that data described by a Landau-Ginzburg equation of state (ie. $\delta = 3$ and $p = 1$ in (13)) yield trajectories of constant β as parallel straight lines, intersecting the y -axis for $\beta < \beta_c$, the x -axis for $\beta > \beta_c$, and the origin for $\beta = \beta_c$.

Overall, the quality of the fit is remarkably good. The only sign of inconsistency is the disagreement in the shape of the curve in the weak coupling phase with $\beta \geq 0.55$, although even in this regime the fit apparently passes close to “centre of mass” of the data. As seen

in Fig. 8, the data here lie below the fit but curve more strongly, which they must do if they are ultimately to intercept the y -axis in the chiral limit.

For $N_f = 4$, we were unable to find any fit of comparable quality. Global fits to all 143 points in the dataset typically yielded a $\chi^2/dof \simeq O(5)$. Since in Fig. 2 the low mass points are clearly finite volume effected, one strategy is to exclude them and only fit to the 42 datapoints with $\beta \leq 0.20$, $m_0 \geq 0.01$, yielding

$$\begin{aligned} A &= 2.27(29) & \delta &= 2.59(18) & \beta_c &= 0.212(4) & \chi^2/dof &= 0.95 \\ B &= 0.60(7) & p &= 0.98(13) \end{aligned} \quad (15)$$

A slightly more satisfactory fit including a wider window in β was found when some attempt at incorporating a finite-volume scaling analysis was made, by modifying the equation of state to [17]

$$m_0 = A((\beta - \beta_c) + CL_s^{-\frac{1}{\nu}})\langle\bar{\chi}\chi\rangle^p + B\langle\bar{\chi}\chi\rangle^\delta, \quad (16)$$

where for the exponent ν we use the hyperscaling prediction

$$\nu = \frac{(\delta + 1)}{3(\delta - 1)}. \quad (17)$$

The best fit to (16) was found for the the 121 datapoints with $0.15 \leq \beta \leq 0.4$, $m_0 \leq 0.015$:

$$\begin{aligned} A &= 1.988(24) & \delta &= 2.653(30) & \beta_c &= 0.2129(8) & \chi^2/dof &= 8.1 \\ B &= 0.451(9) & p &= 1.152(3) & C &= 0.176(7) \end{aligned} \quad (18)$$

Although the χ^2/dof is much higher, this fit does a better job in the ‘‘symmetric’’ phase $\beta \geq 0.4$, and is shown by dashed lines for in Fig. 2, and in Fisher coordinates in Fig. 9 (strong coupling) and Fig. 10 (weak coupling). In any case, the fitted values of the critical parameters do not vary much between (15) and (18).

As for $N_f = 1$, the Fisher plot highlights systematic discrepancies in the symmetric phase. Overall, though, it is difficult to conclude on the basis of this analysis whether chiral symmetry is restored for $N_f = 4$ as $\beta \rightarrow \infty$ or not. There is, however, a significant change in the fitted exponent β_{mag} as N_f changes from 1, where from (14) it has the value 1.20(3), to $N_f = 4$ where it takes the value 0.62(9) (15) or 0.67(1) (18). This trend is consistent with the distinct curvatures of the $\langle\bar{\chi}\chi\rangle_0(\beta)$ data in Fig. 3, and is a more dramatic effect than the increase of $\delta(N_f)$, which even for $N_f = 4$ still lies below the Landau-Ginzburg value.

4 Discussion

Our main result is that there is convincing evidence for spontaneously broken chiral symmetry in the continuum limit in the theory with $N_f = 1$; any extrapolation of the data of Fig. 5 resulting in a vanishing condensate in this limit must rely on a hitherto unobserved curvature close to the chiral limit. The one theoretical framework in which we might understand the origin of such a curvature, namely chiral effective theory, has the assumption of chiral

symmetry breaking built in. Therefore we can say with some confidence that $N_{fc} > 1$, and with slightly less confidence that the dimensionless condensate $\beta^2 \langle \bar{\psi} \psi \rangle \sim O(10^{-3})$.

For $N_f = 4$ the situation is much less clear cut. We could not possibly hope to confirm $N_{fc} > 4$ by direct simulation using current resources, since even for $N_f = 2$ the dimensionless condensate, if there, is too small to measure [6]. We have instead contrasted $N_f = 4$ with $N_f = 1$ by treating the passage from strong to weak coupling as if there were a true phase transition, and attempted to characterise the equation of state by critical exponents. It is somewhat ironic that this proved quite successful for $N_f = 1$ where we believe there is no transition but merely a crossover; indeed the quality of the fit is if anything superior to similar fits obtained in systems where a true phase transition is believed to occur (eg. [17, 28, 18]). For $N_f = 4$ the fits are less compelling, although this could merely reflect a less comprehensive dataset. The only significant difference between the two theories is in the exponent β_{mag} , which halves as N_f increases from 1 to 4. There is also a small increase in δ from 2.3 to 2.7, which should be contrasted with the chiral symmetry restoring transition in the 2+1d Thirring model (which has the same global symmetries as QED₃ in both lattice and continuum theories), which for $N_f = 2$ has $\delta \simeq 2.7$, increasing to 3.1 for $N_f = 3$, 3.4 for $N_f = 4$, and finally to $\gtrsim 4$ for $N_f = 5$ [17, 18, 19] (data for the Thirring model with $N_f = 1$ do not exist). Of course, the hypothesis that the two models have a common fixed point behaviour implying the exponents should coincide only holds for $N_f = N_{fc}$. Naively one might deduce from the trends in these numbers that this would occur for $N_f < 2$; however, one should bear in mind that the equivalence should only hold for Thirring transitions at $G^2 = \infty$ and QED transitions at $\beta = \infty$. In the Thirring case there is some ambiguity about identifying the strong coupling limit using a lattice regularisation [17], and it is unlikely that such information about QED could ever emerge from a numerical simulation, though of course, it may be an interesting question to address for analytic approaches. It is also interesting to speculate about the nature of the universality class of the transition at finite β_c for $N_f > N_{fc}$, in particular the question of whether it is governed by the global symmetries of the continuum or the lattice model.

Acknowledgements

SJH was supported by a PPARC Senior Research Fellowship, and thanks the Institute for Nuclear Theory at the University of Washington for its hospitality and the Department of Energy for partial support during the completion of this work. JBK is supported in part by NSF grant PHY-0102409. The computer simulations were done on the Cray SV1's at NERSC, the IBM-SP at NPACI, the SGI Origin 2000 at the University of Wales Swansea, and on PCs at DESY Hamburg and Humboldt Universität Berlin. We have enjoyed discussions with Shailesh Chandrasekharan, Valery Gusynin, Igor Herbut, Nick Mavromatos, Manuel Reenders, Rohana Wijewardhana, Pieter Maris and Zlatko Tešanović.

References

- [1] R. D. Pisarski, Phys. Rev. D **29** (1984) 2423.
- [2] T. Appelquist, D. Nash and L. C. R. Wijewardhana, Phys. Rev. Lett. **60** (1988) 2575; M.R. Pennington and S.R. Webb, Brookhaven preprint BNL-40886; M. R. Pennington and D. Walsh, Phys. Lett. B **253** (1991) 246; P. Maris, Phys. Rev. D **54** (1996) 4049 [arXiv:hep-ph/9606214].
- [3] E. Dagotto, A. Kocić and J.B. Kogut, Phys. Rev. Lett. **62** (1989) 1083; Nucl. Phys. **B334** (1990) 279;
- [4] V. Azcoiti and X. Q. Luo, Mod. Phys. Lett. A **8** (1993) 3635 [arXiv:hep-lat/9212011]; J. Alexandre, K. Farakos, S. J. Hands, G. Koutsoumbas and S. E. Morrison, Phys. Rev. D **64** (2001) 034502 [arXiv:hep-lat/0101011].
- [5] S. J. Hands and J. B. Kogut, Nucl. Phys. B **335** (1990) 455.
- [6] S. J. Hands, J. B. Kogut and C. G. Strouthos, Nucl. Phys. B **645** (2002) 321 [arXiv:hep-lat/0208030].
- [7] T. Appelquist and L. C. R. Wijewardhana, arXiv:hep-ph/0403250.
- [8] P. Maris, private communication.
- [9] M. Franz, Z. Tešanović and O. Vafek, Phys. Rev. **B66** (2002) 054535 [arXiv:cond-mat/0203333].
- [10] I. F. Herbut, Phys. Rev. **B66** (2002) 094504 [arXiv:cond-mat/0202491].
- [11] M. Franz and Z. Tešanović, Phys. Rev. Lett. **84** (2000) 554.
- [12] A. Kovner, B. Rosenstein and D. Eliezer, Mod. Phys. Lett. A **5** (1990) 2733.
- [13] T. Appelquist, A. G. Cohen and M. Schmaltz, Phys. Rev. D **60** (1999) 045003 [arXiv:hep-th/9901109].
- [14] N. E. Mavromatos and J. Papavassiliou, arXiv:cond-mat/0311421.
- [15] D. Espriu, A. Palanques-Mestre, P. Pascual and R. Tarrach, Z. Phys. C **13** (1982) 153; S. J. Hands, Phys. Rev. D **51** (1995) 5816 [arXiv:hep-th/9411016].
- [16] T. Itoh, Y. Kim, M. Sugiura and K. Yamawaki, Prog. Theor. Phys. **93** (1995) 417 [arXiv:hep-th/9411201].
- [17] L. Del Debbio, S. J. Hands and J. C. Mehegan [UKQCD Collaboration], Nucl. Phys. B **502** (1997) 269 [arXiv:hep-lat/9701016].
- [18] L. Del Debbio and S. J. Hands, Nucl. Phys. B **552** (1999) 339 [arXiv:hep-lat/9902014].

- [19] S. J. Hands and B. Lucini, Phys. Lett. B **461** (1999) 263 [arXiv:hep-lat/9906008].
- [20] S. Gottlieb, W. Liu, D. Toussaint, R. L. Renken and R. L. Sugar, Phys. Rev. D **35** (1987) 2531.
- [21] P. Hasenfratz, Nucl. Phys. Proc. Suppl. **106** (2002) 159 [arXiv:hep-lat/0111023].
- [22] V. P. Gusynin and M. Reenders, Phys. Rev. D **68** (2003) 025017 [arXiv:hep-ph/0304302].
- [23] J. Engels and T. Mendes, Nucl. Phys. B **572** (2000) 289 [arXiv:hep-lat/9911028].
- [24] V. P. Gusynin, V. A. Miransky and A. V. Shpagin, Phys. Rev. D **58** (1998) 085023 [arXiv:hep-th/9802136].
- [25] C. Burden and A.N. Burkitt, Europhys. Lett. **3** (1987) 545.
- [26] M. Salmhofer and E. Seiler, Commun. Math. Phys. **139** (1991) 395 [Erratum-ibid. **146** (1992) 637].
- [27] V. A. Miransky and K. Yamawaki, Phys. Rev. D **55** (1997) 5051 [Erratum-ibid. D **56** (1997) 3768] [arXiv:hep-th/9611142].
- [28] S. J. Hands and J. B. Kogut, Nucl. Phys. B **520** (1998) 382 [arXiv:hep-lat/9705015].

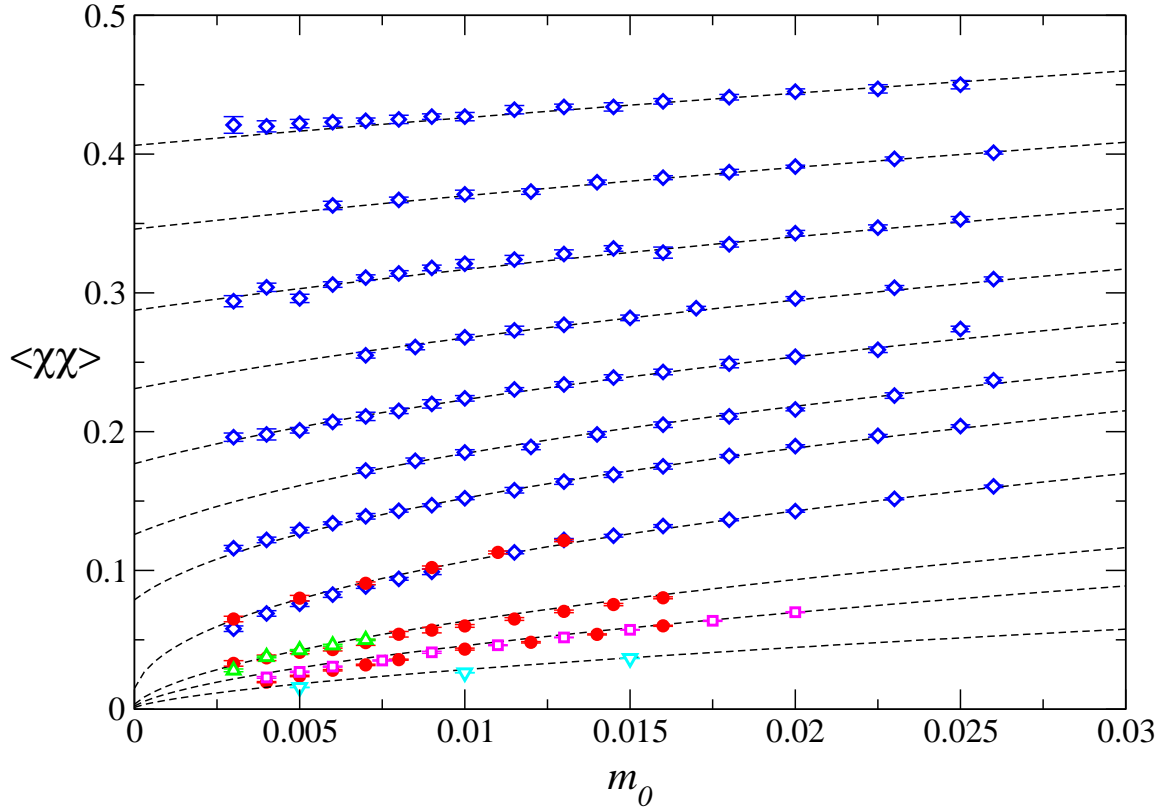


Figure 1: Chiral condensate $\langle \bar{\chi}\chi \rangle$ vs. mass m_0 for $N_f = 1$ from 24^3 (diamonds), 32^3 (filled circles), 44^3 (triangles), 48^3 (squares) and 80^3 (∇) lattices. The lines denote fits to data at constant β to be discussed in Sec. 3.3, for β values (from the top) 0.25, 0.275, 0.3, 0.325, 0.35, 0.375, 0.4, 0.45, 0.55, 0.65 and 0.90.

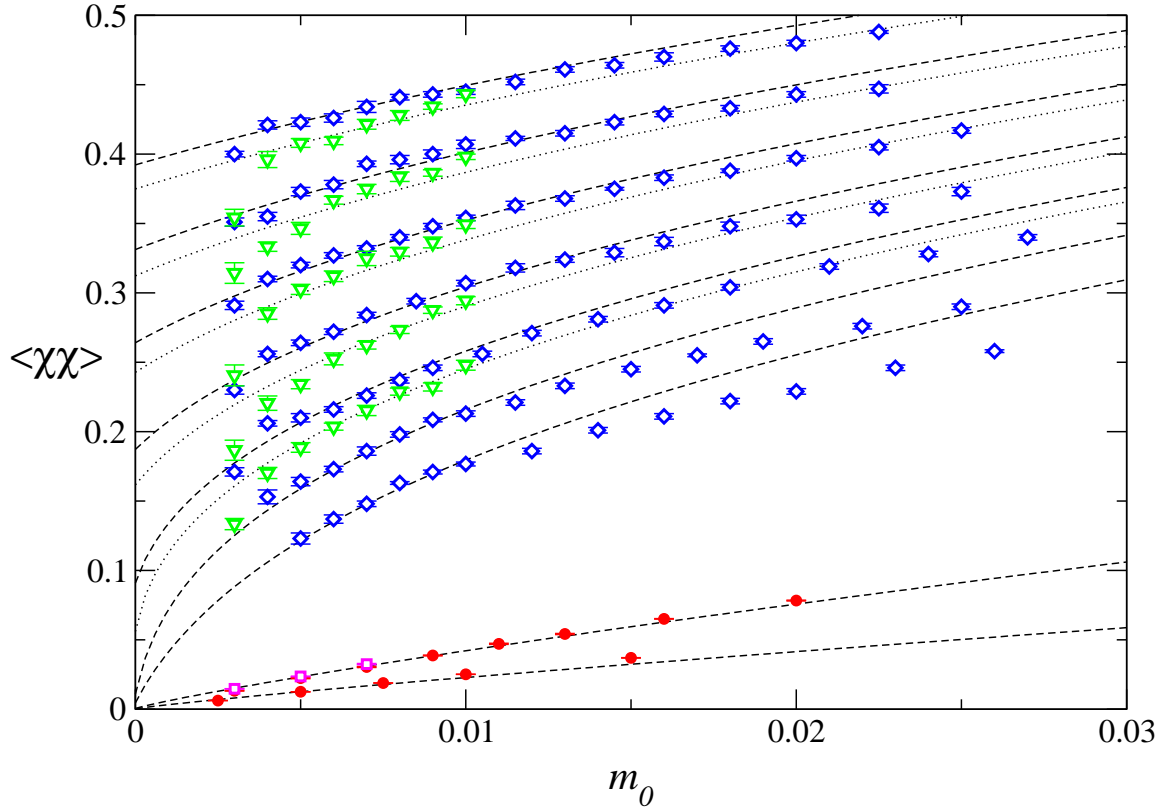


Figure 2: $\langle \bar{\chi}\chi \rangle$ vs. m_0 for $N_f = 4$ from 16^3 (triangles), 24^3 (diamonds), 32^3 (filled circles) and 48^3 (squares) lattices. The lines denote finite volume scaling fits to data at constant β (see Sec. 3.3), for β values (from the top) 0.15, 0.1625, 0.175, 0.1875, 0.2, 0.2125, 0.225, 0.4 and 0.6, with dotted lines denoting fits to 16^3 and dashed lines fits to all other volumes.

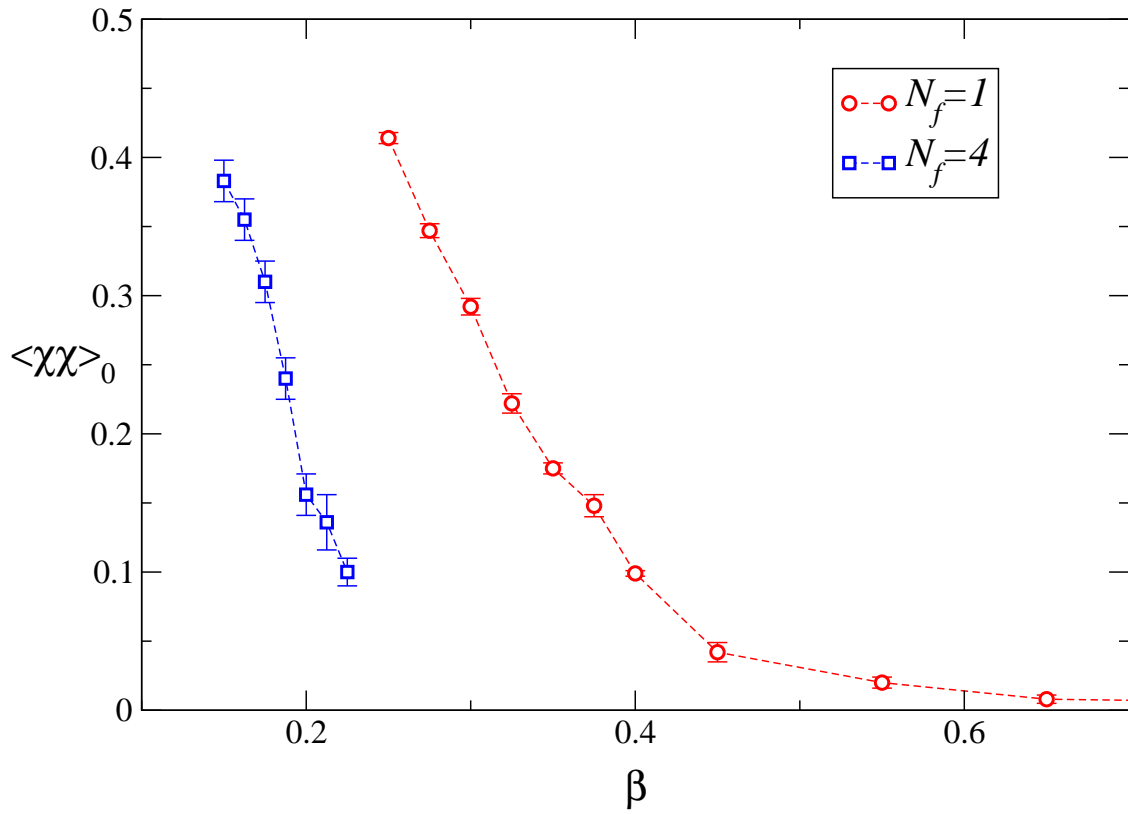


Figure 3: The value of $\langle \bar{\chi}\chi \rangle$ obtained in the chiral limit vs. β

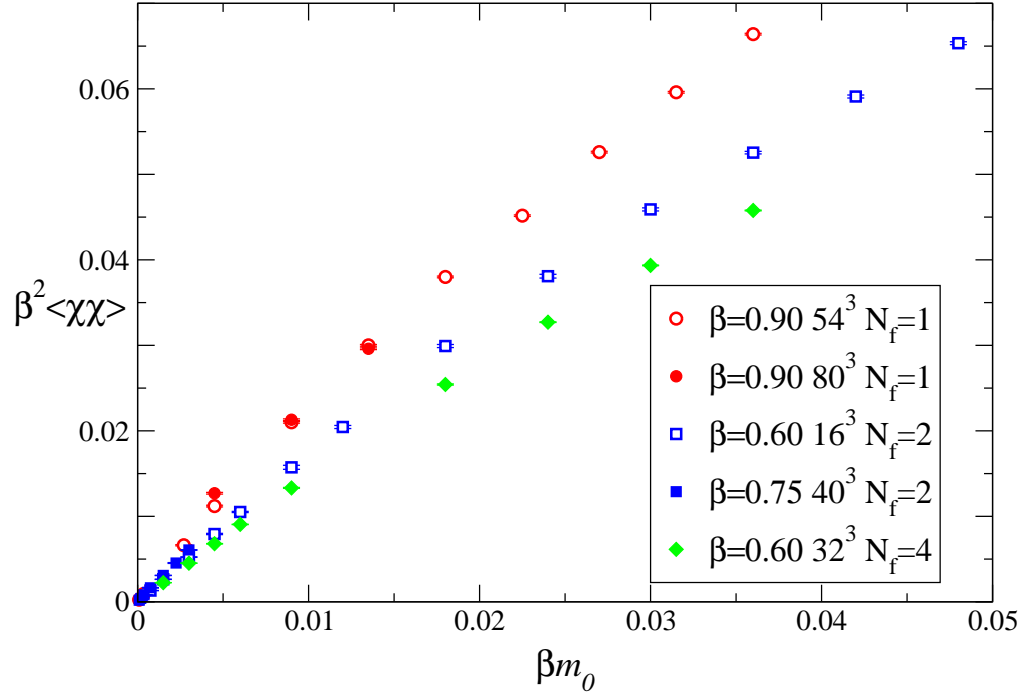


Figure 4: $\beta^2 \langle \bar{\chi} \chi \rangle$ vs. βm_0 for $N_f = 1, 2$ and 4 for the datasets closest to continuum and chiral limits.

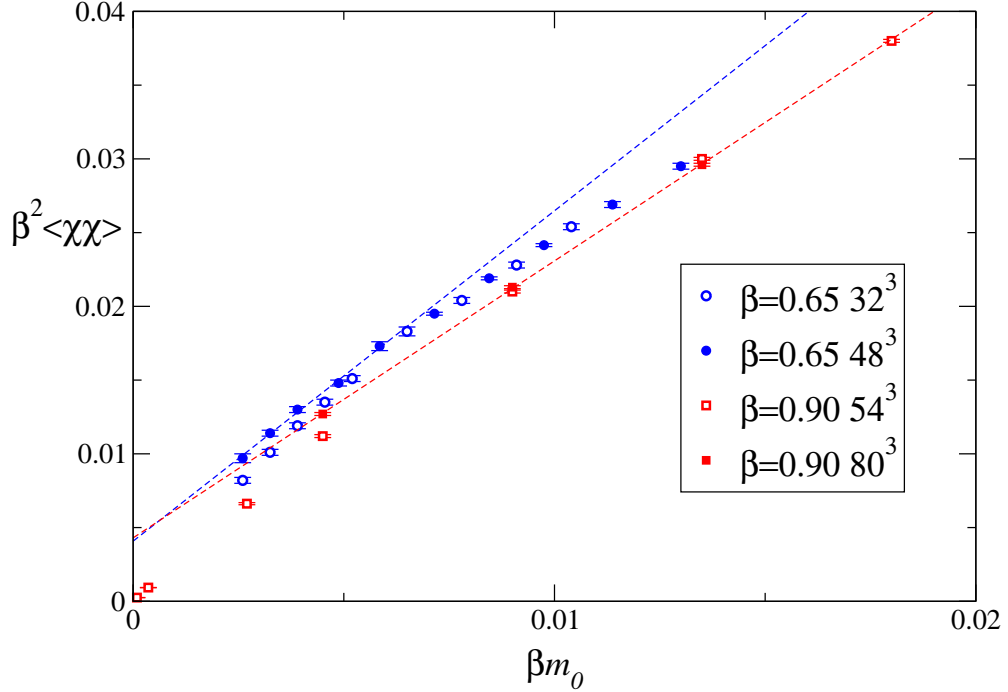


Figure 5: $\beta^2 \langle \bar{\chi} \chi \rangle$ vs. βm_0 for $N_f = 1$ in the region of the chiral limit.

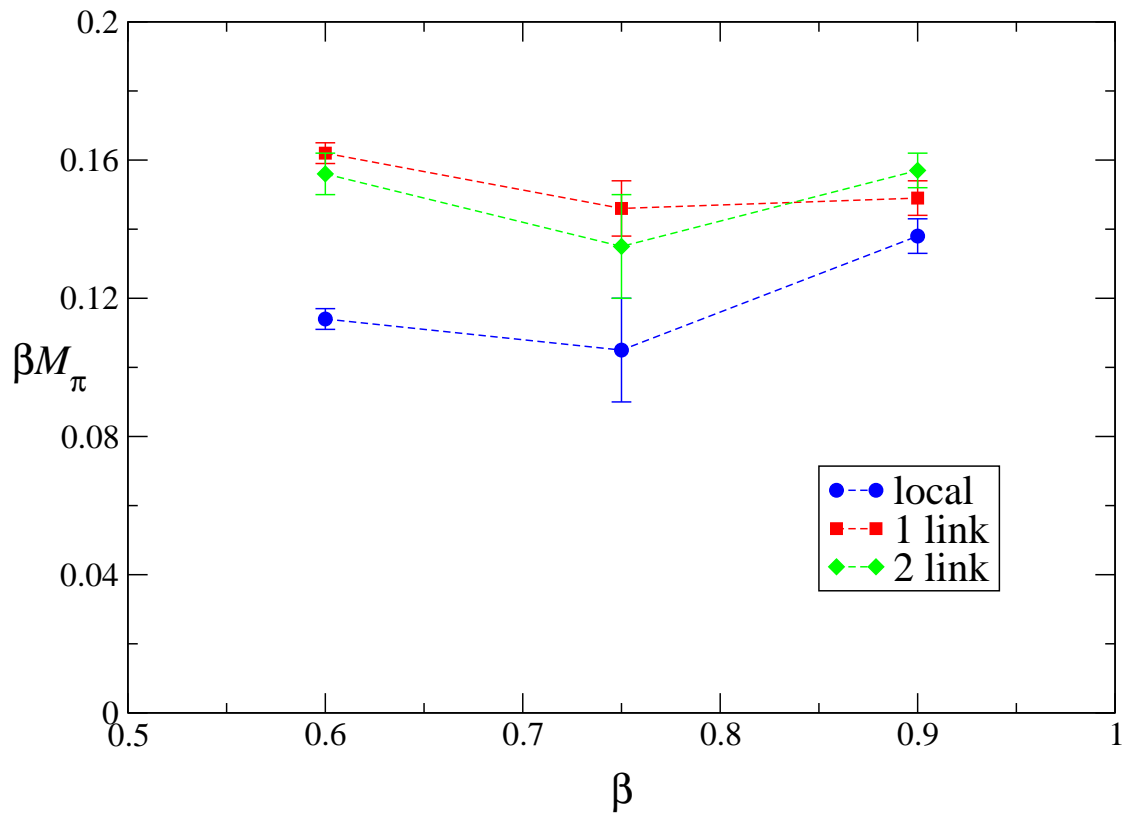


Figure 6: Dimensionless masses βM_π vs. β for the various pion operators discussed in Sec. 3.2.

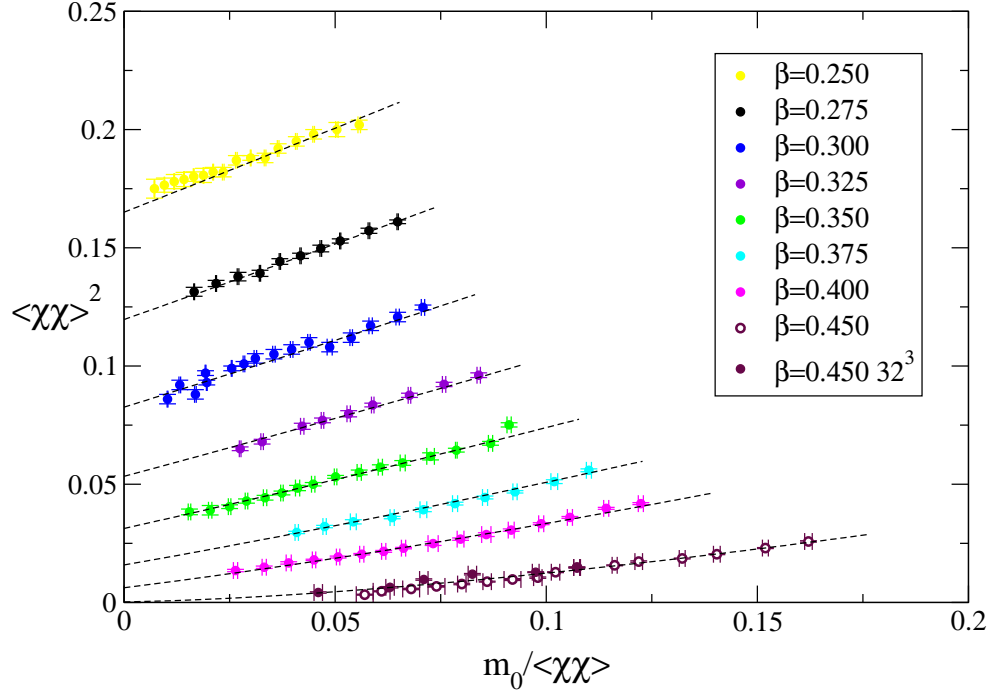


Figure 7: Fisher plot $\langle \bar{\chi} \chi \rangle^2$ vs. $m_0 / \langle \bar{\chi} \chi \rangle$ for strong coupling data with $N_f = 1$. Unless stated all data are from 24^3 lattices. The dashed lines are the result of the fit (14).

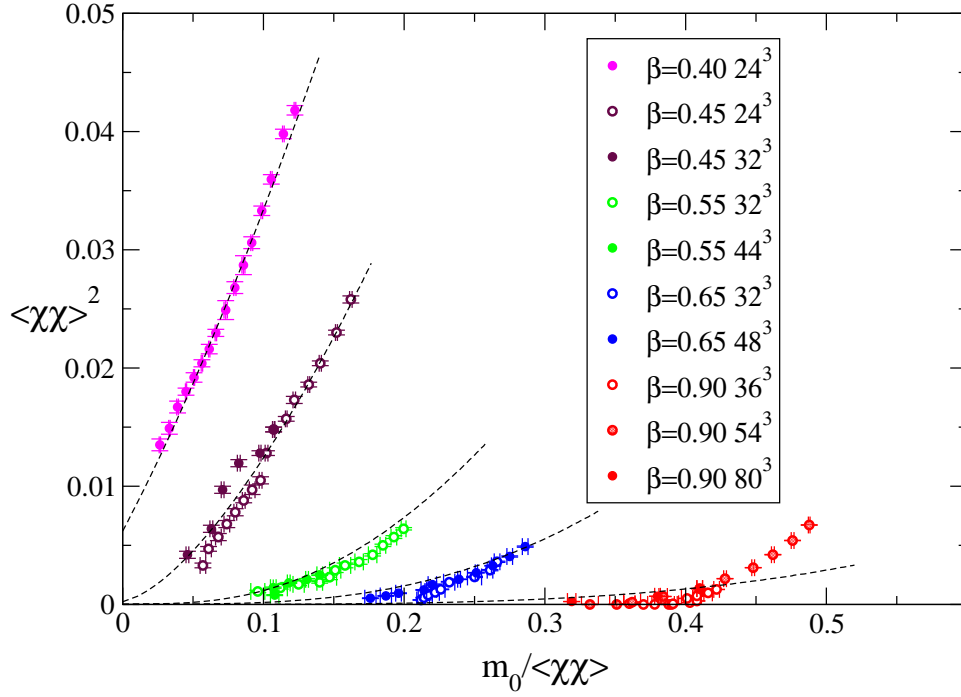


Figure 8: Fisher plot for weak coupling data with $N_f = 1$.

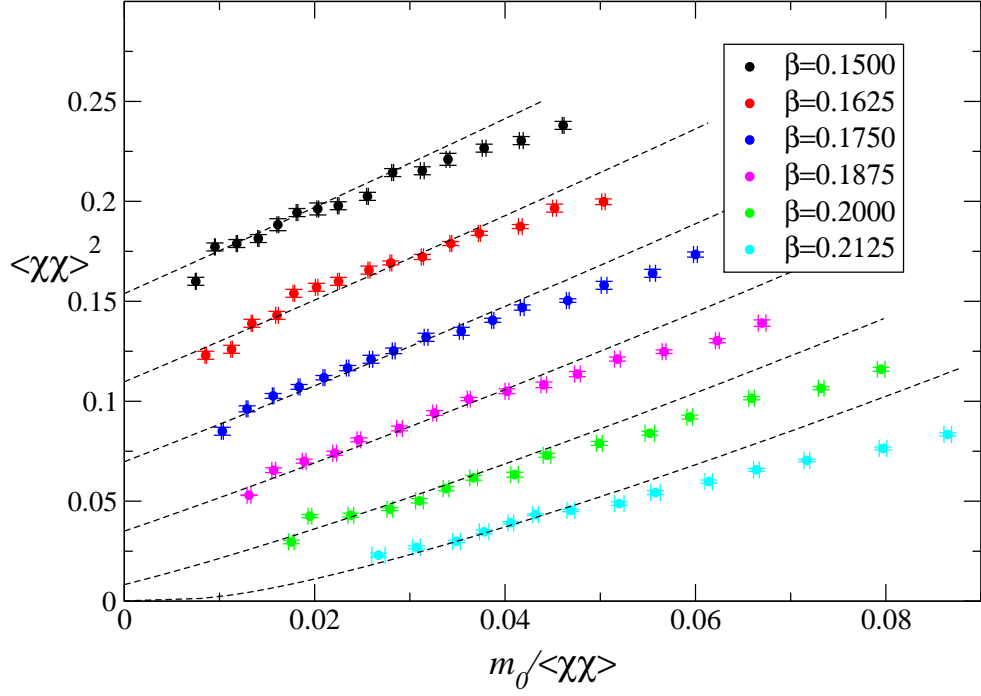


Figure 9: Fisher plot of the strong coupling data from a 24^3 lattice for $N_f = 4$; the dashed lines are the result of the fit (18).

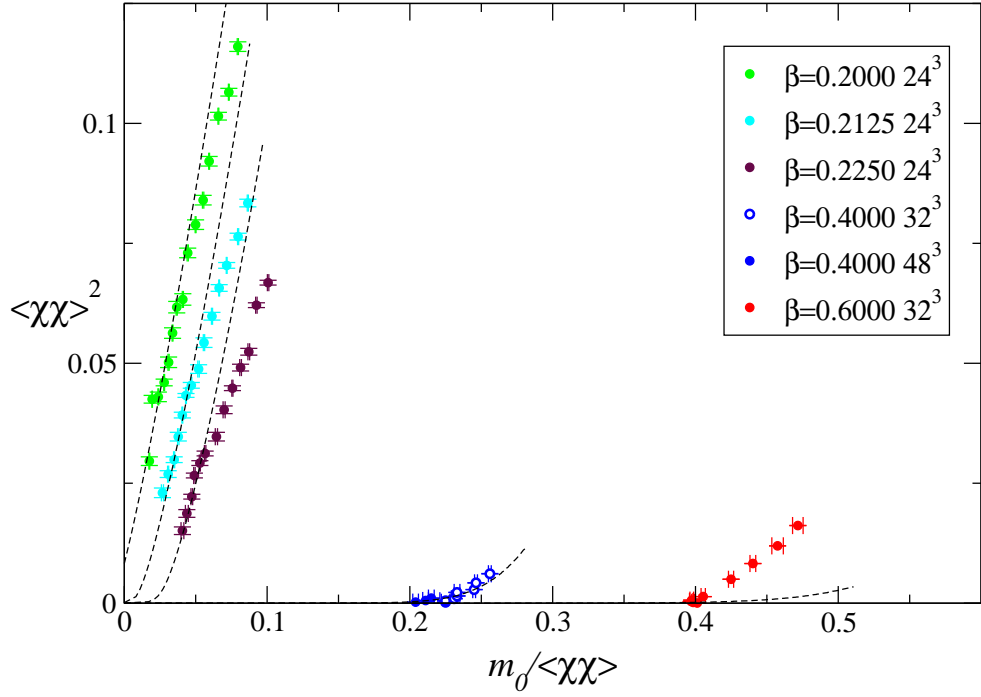


Figure 10: Fisher plot of the weak coupling data for $N_f = 4$.